PROGRESS ON THE RESEARCH OF THERMAL-HYDRAULICS FOR SCWR IN CIAE

Chen Yuzhou, Yang Chunsheng, Zhao Minfu, Du Kaiwen, Zhang shuming
China Institute of Atomic Energy, Beijing, China

Abstract

The experimental data on critical flow, heat transfer and critical heat flux have been obtained at the test loop of supercritical water in China Institute of Atomic Energy. The major characteristics and parametric trends of these phenomena are presented, and the experimental results are compared with the calculations of existing correlations and models.

1. Introduction

In recent years the Supercritical Water Cooled Reactor (SCWR) has been selected as a candidate for generation-IV nuclear power system due to its high thermal efficiency and considerable simplification. The thermal-hydraulics is a major challenge for the R&D of the SCWR due to the complexities in the phenomena and lack of experimental data for supercritical water. In China Institute of Atomic Energy (CIAE) a supercritical water loop was constructed for the experiments of the critical flow, heat transfer and critical heat flux. So far, a large number of experimental data of critical flow and some preliminary results on the heat transfer and critical heat flux have been obtained. In this report the major characteristics of the phenomena are presented and the experimental data are compared with the existing physical models or correlations.

2. Experimental facility

Fig.1 shows the diagram of the supercritical water loop for critical flow experiment. It consists of a three-head piston pump, a dumping tank, a preheater, a condenser, heat exchangers and valves, etc.. The maximum pressure is 30 MPa and the flow rate is 2400 kg/h. The power capacity is 75V×15000 A DC. With this system the experiment is conducted at stable condition. With some minor modifications this loop is also used for experiments of heat transfer and critical heat flux.

3. Critical flow

Two nozzles, A and B, as shown in Fig.2, were tested. They had 1.41 mm in diameter and 4.35 mm in length with rounded-edge of r = 1mm and sharp-edge, respectively. More than 250 experimental data were obtained, covering the ranges of pressures of 22.1 – 29.1 MPa and inlet temperatures of 38 – 474 □ .

3.1 Experimental results

The experimental results are shown in Fig. 3 by displaying G_M versus DT_{PC} (= $T_{PC} - T_0$) , where

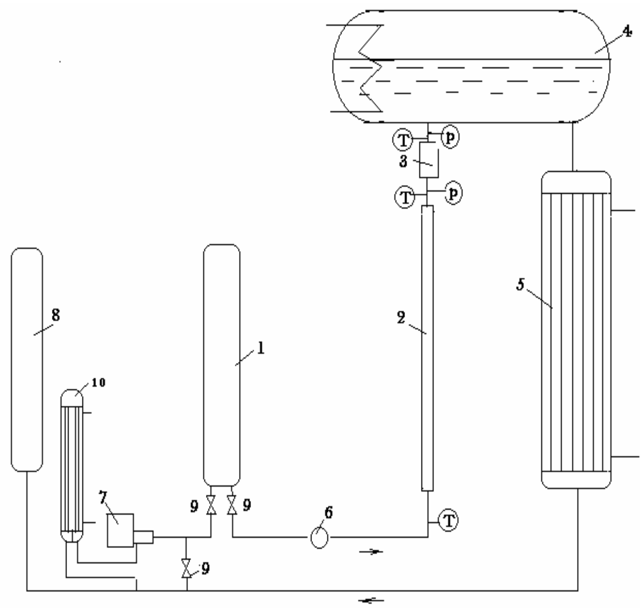

Figure.1 Diagram of supercritical water loop for critical flow experiment

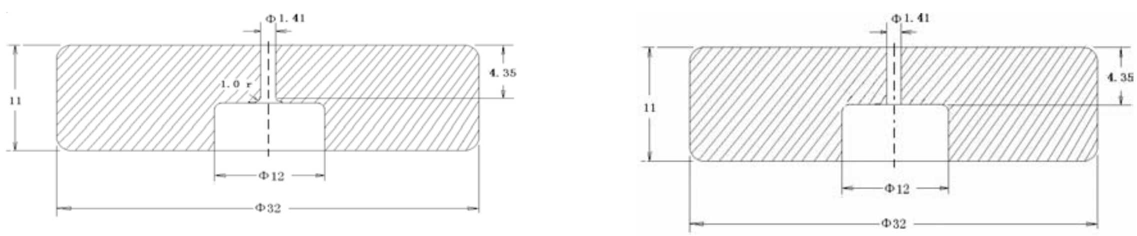

(a) Nozzle A (b) Nozzle B

Figure 2 Schematic of nozzle test sections

G_M is the measured mass flux, T_0 the inlet bulk temperature, and T_{PC} the pseudo-critical temperature. The results of two nozzles are compared in Fig.4.

As seen, the mass flux decreases as DT_{PC} decreasing (or inlet temperature increasing). The trend is moderate in the regions of beyond T_{PC} ($DT_{PC} <0$) and well below T_{PC} (i.e. DT_{PC} larger than about 100 K), while it varies sharply in the near pseudo-critical region.

In the region of $DT_{PC} > 0$ (> 30 K in particular) the data points appear scattered from the general trend, characterized by a kind of instability. This behavior seems relative to the experimental procedure. The test started from a low temperature, and proceeded by increasing temperature run by run toward the pseudo-critical temperature. In this period the flow rate decreased smoothly as the temperature increasing. Then the test was repeated by decreasing the temperature. In this period the flow exhibited very slow excursion, and lower flow rates were generally attained, compared to those obtained in the former period for the same p_0 and T_0. This behavior was more

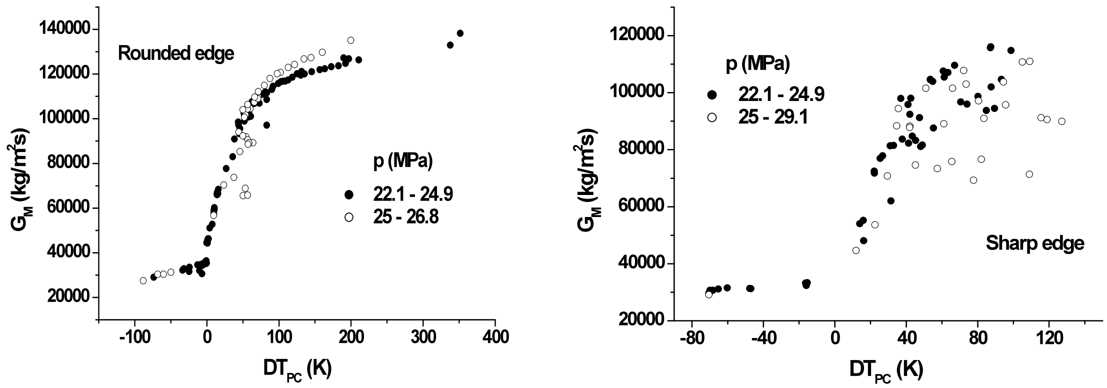

(a) Nozzle A (b) Nozzle B

Figure 3 Variations of measured mass flux with DT_{PC}

predominant for nozzle B, especially at higher pressure. In the region of $DT_{PC} < 0$ it appeared not obvious and the results of two nozzles were not different appreciably. This effect can be explained in terms of the local resistance and the onset of vaporization. In the region of $DT_{PC} < 0$ the local resistance at the inlet only takes a small fraction of the overall resistance. The onset of vaporization is related with the region of $DT_{PC} > 0$, and it is closely related to the inlet shape, as will be discussed latter.

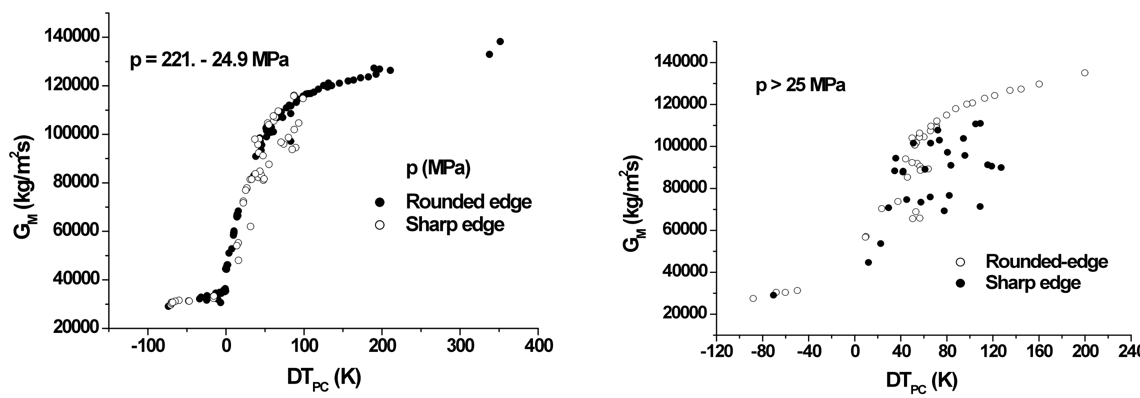

(a) (b)

Figure 4 Comparison of the measured results between two nozzles

3.2.Analysis

3.2.1 Onset of vaporization

The critical flow is dominated by the vapor content strongly, and thus is closely related with the onset of vaporization. It is recognized that the drastic subcooled depressurization is a non-equilibrium process, and the vaporization would occur at a superheat, i.e., the first nucleation would occur at a pressure, p_n, lower than the local saturation pressure, p_s. The pressure difference, p_s - p_n, as called pressure undershoot [1], is increased as the depressurization rate increasing (or as the temperature decreasing). For p_0 = 25 MPa and DT_{PC} = 60K, for instance, it is estimated to be around 6 MPa, corresponding to a superheat of as high as about 50 K. It decreases as DT_{PC} decreasing, and is about 20 K for DT_{PC} = 30K.

Furthermore, the velocity and pressure in the throat are not uniform. Fig.5 illustrates the pressure distributions in liquid-phase flow calculated by CFD for two nozzles. As seen, for sharp-edge the non-uniformity of the pressure at a cross section is much severer than rounded-edge. A minimum pressure exists near the inlet of throat, which is determinant for the vapor generation.

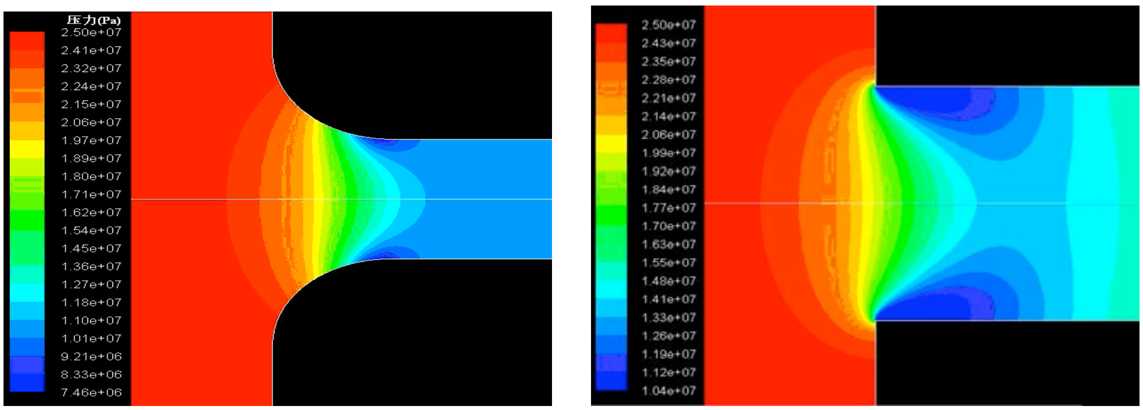

(a) Nozzle A with rounded-edge (r = 1 mm)
p_0 = 25 MPa, G = 164600 kg/m^{2}s

(b) Nozzle B with sharp-edge
p_0 = 25 MPa, G = 97500 kg/m^{2}s

Figure 5 Pressure distributions in two nozzles

In general, the onset of vaporization is related with the depressurization rate, the experimental procedure, and even the surface imperfection, dissolved gas or suspended particle in the liquid, etc.. Therefore, the superheat could be rather large for the first bubble formation. But once the nucleus is activated the bubble could be generated at a small superheat. Furthermore, the vaporization is accompanied by an increase in the local resistance, which produces a positive feedback effect to enhance the vaporization further and to decrease the flow rate even at a decreased temperature.

3.2.2 Instability and bifurcation behavior

As discussed above , and the superheat for the onset of vaporization is dependant on variety of factors, and may vary significantly for same inlet pressure and temperature, associated with great uncertainty in the vapor generation and flow rate.

Fig.6 illustrates a result calculated by a modified homogeneous equilibrium model (as will be described latter). Firstly, the calculations are performed successively as temperature increasing step by step. In this period, considering the pressure undershoot the vaporization is not predicted to occur at the inlet of throat until the temperature closes to T_{PC}. Then, the calculations are repeated successively as temperature decreasing step by step. In the latter period the nucleus is assumed activated, and the superheat for vaporization is not considered (i.e. p_n = p_s). As seen, lower results are calculated than those in the first period, and a bifurcation behavior is produced, characterizing a kind of instability. This calculation explains qualitatively the scattered feature in the region of $DT_{PC} > 0$. It should be noted that in the calculations the local resistance is simply based on single liquid-phase flow. Actually, after the onset of vaporization the local pressure loss would increase, and the difference in the results between two periods could be even larger.

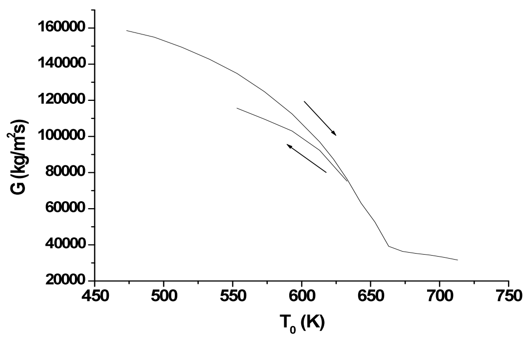

Figure 6 Illustration for the instability of mass flux due to uncertainty in the onset of vaporization ($p_0 = 25$ MPa)

The onset of vaporization would take place at DT_{PC} larger than a certain value and the inlet pressure at throat below subcritical pressure. For the nozzle with sharp-edge the significant pressure non-uniformity would associate with greater uncertainty in the onset of vaporization and thus severer instability, compared to rounded-edge. While in the region of near or beyond pseudo-critical temperature this effect is less important and the instability for both nozzles is not obvious.

\3.3Prediction of mass flux

3.3.1 Critical flow

In the previous experiments it was concluded that under subcritical pressure condition the thermal non-equilibrium tended to decrease as pressure increasing, and thermal equilibrium was dominant at supercritical pressure [2, 3]. Same finding was achieved in the similar experiments of supercritical water [4] and CO_2 [5].

In the present study, to account for the effect of inlet resistance the Homogeneous Equilibrium Model (HEM) [3] is modified as

$$G = \left[\frac{2(h_0 - xh_g - (1-x)h_l)}{\frac{C}{\overline{\rho}^2} + (\frac{1-x}{\rho_l} + \frac{x}{\rho_g})^2} \right]^{1/2} \tag{1}$$

where h is the enthalpy, ρ the density, x the equilibrium quality at the critical plane, and the subscripts g and l refer to vapor and liquid, respectively, 0 refers to the stagnation condition, and

$\bar{\rho}$ the average density at the inlet of throat. The mass flux is predicted by Eq. (1) as the downstream pressure decreased successively, until a maximum value is attained and it is taken as the critical mass flux.

3.3.2 Non-critical flow

At certain subcooling the liquid is not vaporized before leaving the throat, and the flow is not choked but is restricted by the flow resistance. Thus, the mass flux is evaluated by the Bernoulli equation, as

$$G = C_D \sqrt{2\rho(p_0 - p_b)}, \tag{2}$$

where p_0 is the inlet pressure; p_b, the back pressure, ρ the water density and C_D is the discharge coefficient.

3.3.3 Estimation of the mass flux

Fig.7 exemplifies the experimental results by G ~ DT_{PC}, and the calculations by the M-HEM (i.e. Eq.(1)) and the Bernoulli equation are superimposed. For the near and beyond pseudo-critical region the instability is not obvious due to less uncertainty in the vaporization, and the M-HEM gives better prediction of the critical flow rate. For DT_{PC} larger than a certain value the instability behavior can not be calculated by the model due to great uncertainty in the onset of vaporization. At assumption of no vaporization at the inlet of throat (i.e, $\bar{\rho} = \rho_l$) the model gives basically the upper envelop of the scattered data. For the nozzle with rounded-edge, at lower pressure the instability is not appreciable over the whole range of temperature, as seen in Fig.7(b), the results are reasonably represented by.

$$G = \mathrm{Min}\,(G_{\text{M-HEM}}, G_{\text{Bernoulli}}) \tag{3}$$

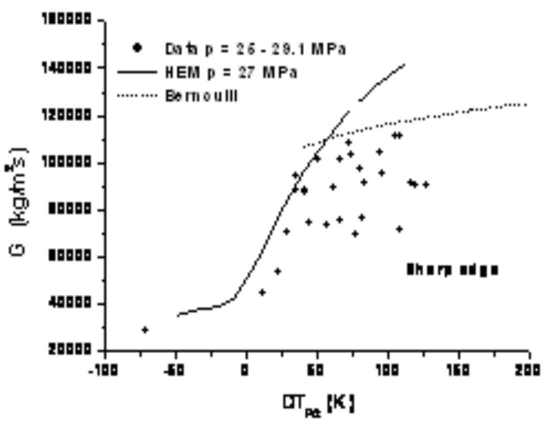

(a) Nozzle B

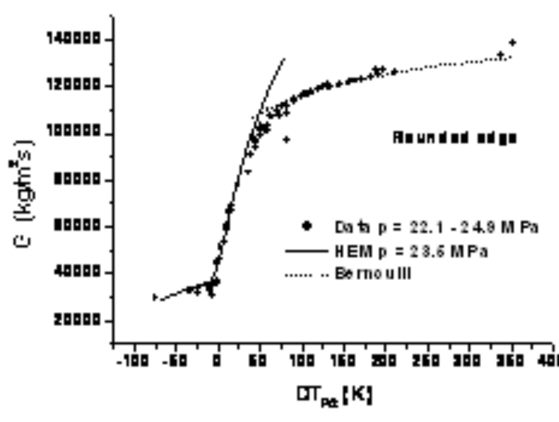

(b) Nozzle A

Figure 7 Comparison of the experimental results with calculations for wider range of DT_{PC}

3.4 Summary

- Flow rate decreases as the inlet temperature increasing, and it varies sharply when the temperature decreases below pseudo-critical point.

- In the region of near or beyond pseudo-critical point the thermal equilibrium is dominant, and the critical flow rate can be estimated reasonably by the modified Homogeneous Equilibrium Model.

- In the region of DT_{PC} larger than a certain value, the critical flow is characterized by some instability, and the inlet shape of nozzle has a substantial effect.

- At the inlet temperature well below the pseudo-critical temperature the choking condition does not take place.

4. Heat transfer

The test section is a stainless-steel tube of 6.07 mm in diameter and 1.3 m in heating length with water flowing upward inside, as shown in Fig.8. The wall temperatures are measured by thermocouples at three locations. The heat loss of the test section is prevented by installing three AC heaters surrounded the tube. The test section is heated by a DC supply.

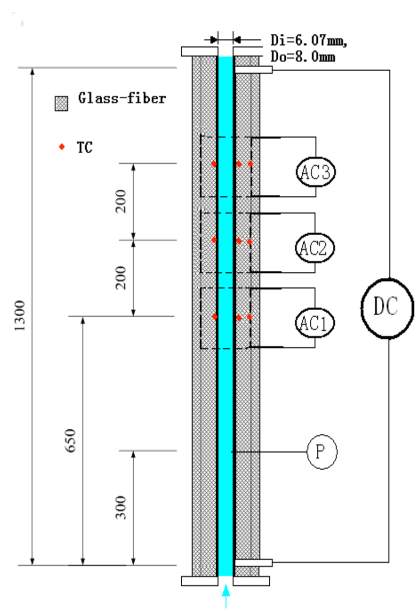

Figure 8 Schematic of heat transfer test section

The experimental parameters cover the ranges of pressure of 10 – 23 MPa, mass flux of 288 – 1298 kg/m^2s, local water temperature of 78 – 270 ℃, heat flux of 0.23 – 1.18 MW/m^2 and Reynolds number of $5.5\times10^3 – 3.9\times10^4$.

4.1 Experimental Results

Fig.9 shows the comparison of experimental results with Dittus-Boelter correlation. For subcritical pressure, at higher Reynolds number the data are predicted by the correlation reasonably. When the Reynolds number decreases to a certain value (i.e., $Re_b < 12000$) the data depart from the correlation sharply. For supercritical pressure, the agreements are mostly within 20%, and distinctly deteriorated heat transfer is observed at two points with wall temperatures above the pseudo-critical temperature.

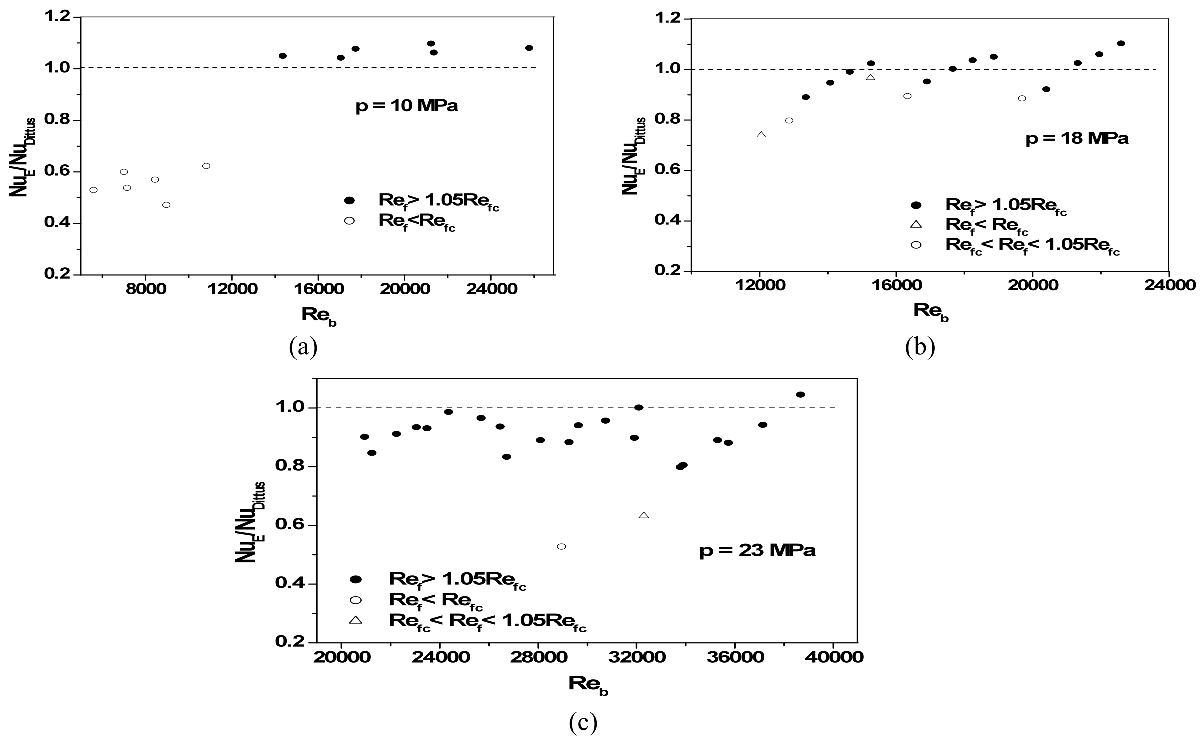

Figure 9 Comparison of experimental data with Dittus-Boelter correlation
(Re_{cf} , see Eq.(6) [13])

In Fig.10 the experimental results are compared with four supercritical heat transfer correlations, including (a) Bishop correlation [7], (b) Jackson correlation [8], (c) Swenson correlation [9] and (d) Yamagata correlation [10]. As seen, except for the two points with $T_W > T_{PC}$, the agreements for the Bishop correlation, Swenson correlation and Jackson correlation are mostly within 10%, while the deviations are slightly increased for Yamagata correlation. The occurrence of deteriorated heat transfer is not predicted by Jackson correlation and Yamagata correlation, but is predicted by the Bishop correlation and Swenson correlation, though the values of Nusselt number are not predicted properly.

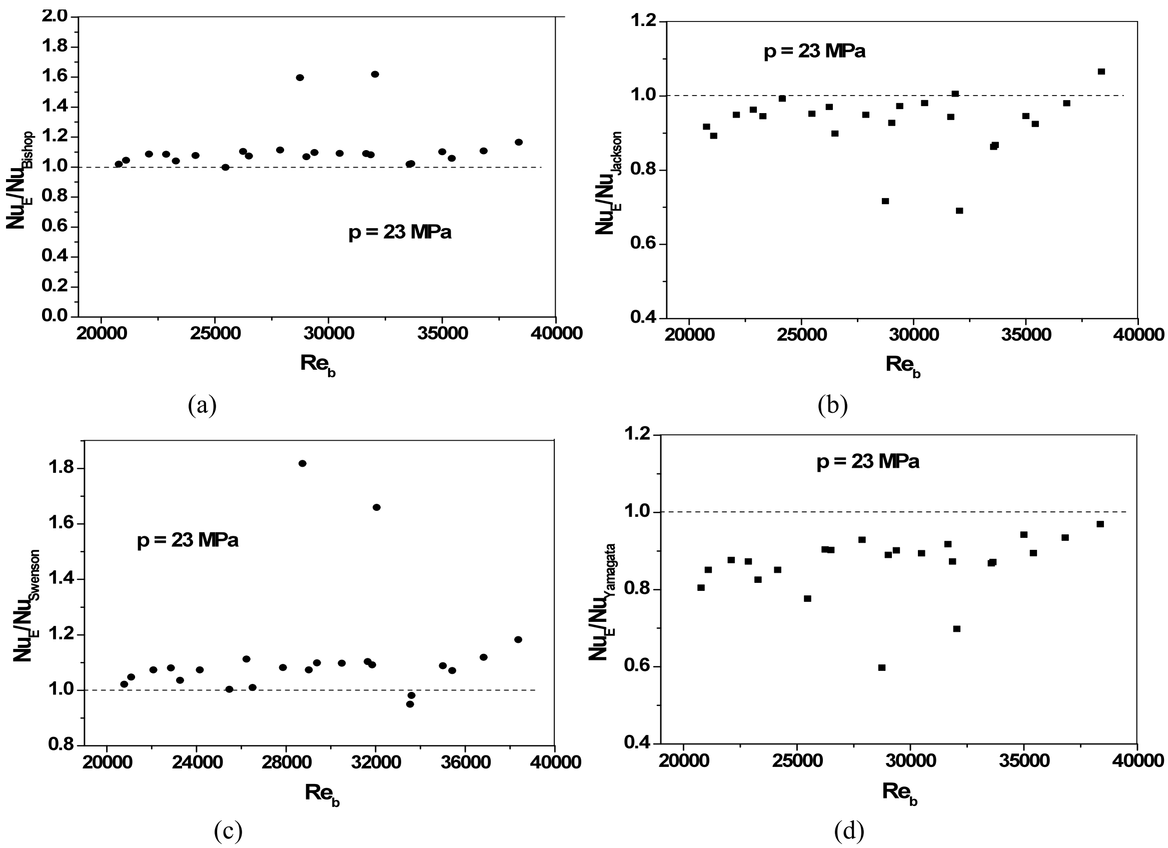

Figure10 Predictions of experimental data by supercritical heat transfer correlations

4.2. Occurrence of deteriorated heat transfer

Two types of deteriorated heat transfer are reported to exist at supercritical pressure. The first one occurs when the wall temperature exceeds the pseudo-critical temperature and thus the wall is covered by vapor. The second one occurs due to the change in flow structure.

From various experiments the occurrence of deteriorated heat transfer was formulated by a relation, $q_c/G = C$, with the value of C ranging from 0.4 – 1.05 kJ/kg [11], and by $q_c = 0.2G^{1.2}$ [10]. This kind of relation is dimensional and does not include some important parameters, e.g. the local fluid temperature and geometry, and it appears not applicable for the present experiment.

To consider the effect of buoyancy force on the flow structure, the following parameter was introduced by Grabezhnnaya and Kirillov [12]

$$k = \left(1 - \frac{\rho_w}{\rho_b}\right)(Gr/\mathrm{Re}_b^2) \tag{5}$$

With

$$Gr = gD^3(\rho_b - \rho_w)/(\rho_b \nu_b^2)$$

For k > 0.01 the effect of buoyancy is assumed appreciable. While for k < 0.01 it is assumed negligible and the heat transfer is estimated with a normal turbulent convection correlation. As seen in Fig.11, for p = 23 MPa the two points with deteriorated heat transfer lay above the line, k = 0.01, while for p = 10 MPa the deteriorated heat transfer, which is attained at $Re_b < 12000$, is represented by a lower limit of k.

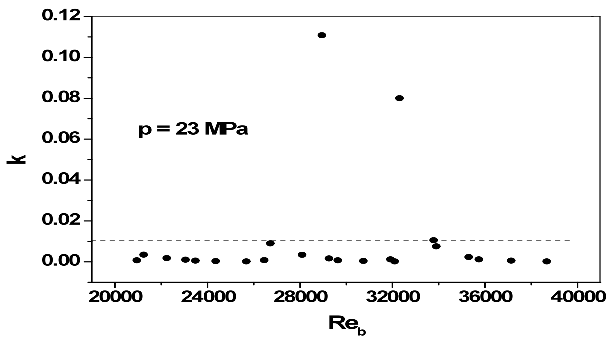

(a)

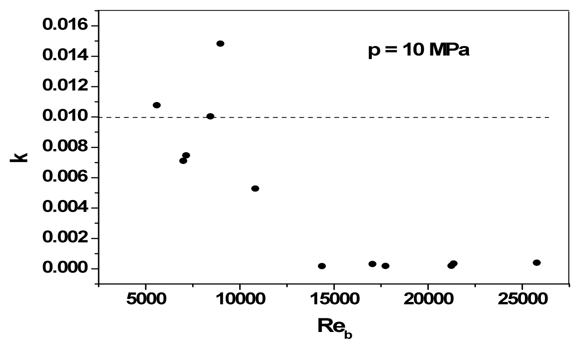

(b)

Figure 11 Parameter k for the data points of p = 23 and 10 MPa

In a heated upward flow the buoyancy force could make a reduction of the shear-stress in the near-wall region, associated with the laminarization and delay in the transition of flow regime from mixed convection to turbulent convection. For the transition between these two regimes, a criterion of critical Reynolds number, Re_{fc}, was derived by Tanaka et al. [13], as follows,

$$\mathrm{Re}_{fc} = 50 Gr_f^{8/21}, \text{ with } Gr_f = \frac{g\beta(T_f - T_b)D^3}{\nu_f^2} \tag{6}$$

in which the subscript f denotes the properties evaluated at film temperature, $T_f = (T_w + T_b)/2$.

As observed in Fig.9, all the data with deteriorated heat transfer are predicted to be in mixed convection regime for both subcritical and supercritical pressure. This result suggests that a significant delay in the transition of flow regimes due to buoyancy force could be the cause of the substantial deterioration in heat transfer. Apparently, the Dittus-Boelter type correlations with modification for the effect of properties near the wall can not adequatly represent the mechanism of the transition of flow regime and the heat transfer characteristic for this regime.

4.3 Summary

- ○ At both subcritical and supercritical pressures, the deterioration in heat transfer could occur at rather high Reynolds number as a result of the change in flow structure.
- ○ For supercritical pressure the existing Dittus-Boelter type correlations with modification for the variations in properties near the wall give better predictions of the heat transfer for the normal turbulent convection, but they can not predict the deteriorated heat transfer satisfactorily.

5. Critical heat flux

Recently, a preliminary experiment of critical heat flux was conducted in a tube of inner diameter of 8 mm and heating length of 0.8 m with water flowing upward. The parameters covered the ranges of pressure of 8.3 – 16.4 MPa , mass flux of 783 – 1034 kg/m^{2}s and local subcooling of 16.5 – 116 ℃.

Under the present low flow condition the critical heat flux, q_M, ranged from 2.3 to 3.3 MW/m^2, and exhibited a weak effect of the subcooling on CHF. The 95-CHF Look-up table gives general overpredictions of the experimental results, as shown in Fig.12.

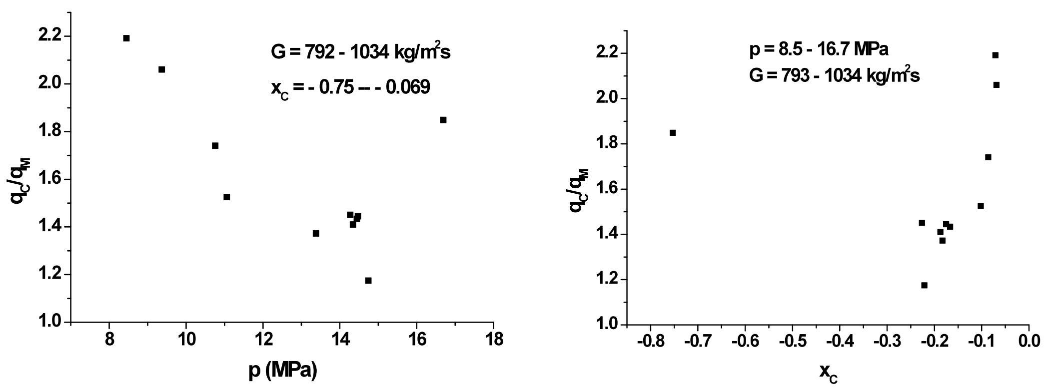

Figure 12 Comparison of CHF experimental data with 95-Look-Up Table

ACKNOWLEDGEMENT

The present study was supported by National Basic Research Program of China (N0. 2007CB209800) and the Coordinated Research Project of International Atomic Energy Agency (IAEA Research contract No. 14469/R0)

REFERENCES

[1] Mid. Alamgir and J.H. Lienhard, "Correlation of pressure undershoot during hot-water depressurization", Trans. ASME, J. Heat Transfer, Vol. 103, 1981, pp.52-55

[2] E.S. Starkman, V.E. Schrock, K.F. Neusen, et al. "Expansion of a very low quality two-phase fluid through a convergent-divergent nozzle". ASME Trans D, J Basic Engineering, Vol. 86, No. 2: 1964, pp.247–256

[3] Chen Yuzhou, Yang Chunsheng, Du Kaiwen, et al. "An experimental study of critical flow of water at steady-state with pressure of up to 22MPa". Proceedings of 7th International Symposium of Heat Transfer, Beijing, 2008

[4] D H. Lee and D. Swinnerton. “Evaluation of critical flow for supercritical steam-water”. NP-3086, 1983

[5] G. Mignot, M. Anderson and M. Corradini, “Measurement and Modelling of Critical Flow for Sopercritical CO_2 Emphasis on Roughness and Diameter Influence”, Proceedings of the 12th International Topical Meeting on Nuclear Reactor Thermal Hydraulics (NURETH-12), LN 111, Sept. 30 – Oct.4 2007, USA

[6] Chen Yuzhou, Yang Chunsheng, Zhang Shuming, Zhao Minfu, Du Kaiwen, “An Experimental Study of Critical Flow of Water under near-critical and Supercritical Pressures”, Proceedings of the 13th International Topical Meeting on Nuclear Reactor Thermal Hydraulics (NURETH-13), N13P1048, Sept. 27 – Oct.3 2009, Japan

[7] A. Bishop, R. Sandberg and L. Tong,， “Forced Convection Heat Transfer to Water at Near-Critical Temperatures and Supercritical Pressures”, WCAP-2056, 1964

[8] J. D. Jackson， “Consideration of the Heat Transfer Properties of Supercritical Pressure Water in Convection with the Cooling of Advanced Nuclear Reactors”， Proceedings of the 13th Pacific Basin Nuclear Conference, Shenzhen City, China, Oct. 21-25, 2002

[9] H. S. Swenson, J. H. Carver and C. R. Kakarala, “Heat Transfer to Supercritical Water in Smooth Bore Tubes”, Trans. ASME, series C, J.Heat Transfer, Vol. 87, No. 4, pp477 – 484, 1965

[10] K. Yamagata, K. Nishigawa, S. Hasegawa, T. Fuju and S. Yoshida, “Forced Convective Heat Transfer to Supercritical Water Flowing in Tubes,” Int. J. Heat Mass Transfer, V15, pp2575-2593, 1972

[11] L. Pioro and R B. Duffey, “Experimental Heat Transfer in Supercritical Water Flowing Inside Channels (survey)”, Nucl. Eng. And Design, 235, pp.2407-2430, 2005

[12] V. A. Grabezhnnaya and P.L. Kirillov, “Heat Transfer under Supercritical Pressures and Heat Transfer Deterioration Boundaries”, Thermal Engineering, V.53, No. 4, pp.296 – 301, 2006

[13]. H. Tanaka, S. Maruyama, and S. Hatano, “Combined forced and natural convection heat transfer for upward flow in a uniformly heated vertical pipe”, Int. J. Heat and Mass Trans. Vol. 30, pp.165-174, 1987